View metadata, citation and similar papers at core.ac.uk

brought to you by CORE

Journal of Physics: Conference Series

PAPER • OPEN ACCESS

The numerical simulation of constrained low-frequency oscillation of a liquid drop

To cite this article: A V Alexandrov *et al* 2019 *J. Phys.: Conf. Ser.* **1158** 022009

View the article online for updates and enhancements.

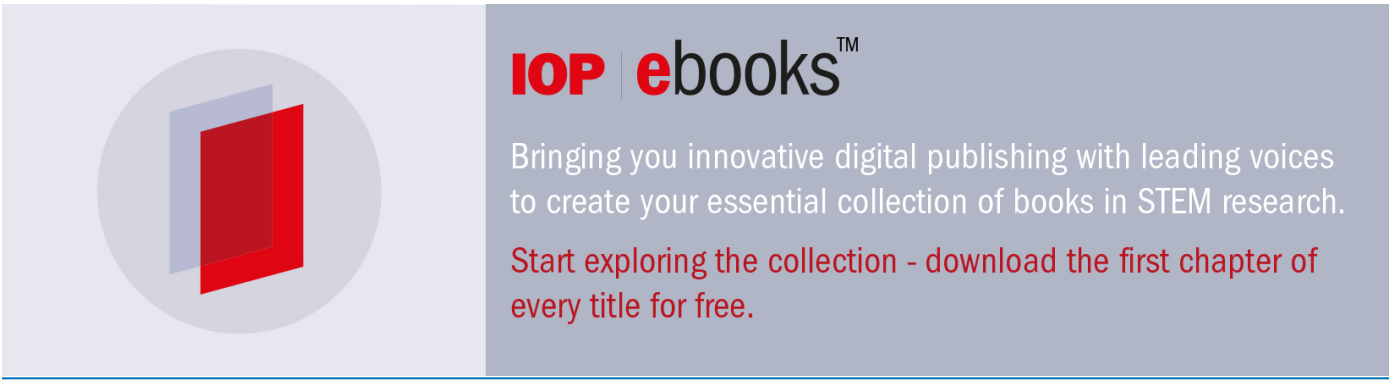

This content was downloaded from IP address 94.25.116.11 on 27/05/2019 at 09:47

The numerical simulation of constrained low-frequency oscillation of a liquid drop

A V Alexandrov[1], I M Kuzmin[1] and L E Tonkov[1, 2]

[1] Institute of Mechanics, Udmurt Federal Research Center, Ural Branch of the Russian Academy of Sciences, 34 T. Baramzimoy, Izhevsk, Russia
[2] Department of Computational Mechanics, Udmurt State University, 1 Universitetskaya, Izhevsk, Russia

E-mail: letonkov@gmail.com

Abstract. The study of microhydrodynamic processes have not only practical significance, but also have a wide field for theoretical approaches and numerical investigation. The amount of accumulated data is large and growing, and allows us to consider the described problem for verification and validation numerical methods and algorithms for capillary flows with a free surface simulation. The feature of the process is the droplet pinning on cylindrical substrate with a cone cavity. The article is concerned with a numerical investigation of constrained oscillation of a liquid drop on a substrate which harmonically oscillates. The discretized form of equation of indicator function advection, after implementing the artificial compression term, leads to cumulative errors of capillary forces due to the unstable calculation of geometric characteristics of the interface surface. The algorithm for computing capillary term of the volume forces is proposed; including iterative regularization when gradient and divergence discrete operators is computed.

1. Introduction

Understanding multiphase flow at low Weber numbers is of considerable importance in a variety of environmental, industrial and engineering applications such as atomization of the fuel, contaminant cleanup, fluid absorption and separation in porous media and many others. However, accurate numerical simulation of such flows is a tricky computational problem when interfacial tension effects become dominant.

Mesh-based numerical methods are conventionally considered as the preferred approach for most applications, however, is the need for an algorithm to determine the shape of interface boundary and its evolution with time.

One of the widespread approaches to solve the investigating problem is representing a bulk as a immiscible incompressible two phase mixture described by Navier–Stokes equations with the dynamic equilibrium condition at the interface and subsequent application algorithm, that represents the interface implicitly by marking the fluids on both sides of the interface, using an scalar indicator function such as a volume fraction α (Volume-Of-Fluid method) [1].

The main advantage of this approach is that it does not require complicated interface tracking algorithms. This is important for modeling two-phase flows through complex geometries with large

Content from this work may be used under the terms of the Creative Commons Attribution 3.0 licence. Any further distribution of this work must maintain attribution to the author(s) and the title of the work, journal citation and DOI.
Published under licence by IOP Publishing Ltd

interface motions and interactions. The surface tension force and the contact angle effect arise from calculation of interface normal vector $\mathbf{n}_s = \nabla\alpha/|\nabla\alpha|$ and curvature $K = \nabla \cdot \mathbf{n}_s$.

The prediction of a liquid droplet natural frequencies and a free surface shapes under constrained oscillations are extensively studied by analytical [2], numerical [3] and experimental [4] methods. Consider these problems as the convenient testing tool of verification and validation numerical methods and algorithms for capillary simulation of the flows with a free surface.

Next we consider a constrained oscillation of a liquid drop on a cylindrical substrate with radius $R = 4$ mm which harmonically oscillates at vertical plane xOy (figure 1). Displacement along axe of symmetry Oy is defined by the harmonic law $h = A\sin\omega t$. The feature of the process is the droplet pinning on substrate with a cone cavity with cone-angle $\beta = 140°$.

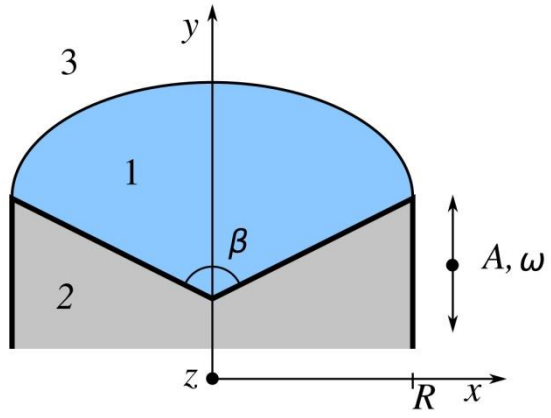

Figure 1. Geometry of the problem: small drop of distilled water (1) located on harmonically oscillated substrate (2) in air (3) environment.

2. Mathematical model and numerical method

The equations of motion for an isothermal, immiscible incompressible two-phase mixture flow of Newtonian fluids can be written using a single-fluid continuum approach as follows:

$$\frac{\partial\rho\mathbf{u}}{\partial t} + \nabla\cdot(\rho\mathbf{u}\mathbf{u}) = -\nabla p + \nabla\cdot\boldsymbol{\tau} + \mathbf{f}_{\mathrm{sv}},\ \nabla\cdot\mathbf{u} = 0, \tag{1}$$

where $\mathbf{u}$ is velocity vector, total pressure p is sum of dynamic and hydrostatic pressure, $\boldsymbol{\tau} = \mu(\nabla u + (\nabla u)^T)$ is viscous stress tensor, $\mathbf{f}_{\mathrm{sv}}$ is surface tension force per unit volume. The density and viscosity are defined by

$$\rho = \alpha\rho_{\mathrm{l}} + (1-\alpha)\rho_{\mathrm{g}},\ \mu = \alpha\mu_{\mathrm{l}} + (1-\alpha)\mu_{\mathrm{g}}, \tag{2}$$

where subscripts "l" and "g" denotes liquid ($\alpha = 1$) and gas ($\alpha = 0$) phase respectively. The scalar indicator function α is evolved with an advection equation of the conservative form:

$$\frac{\partial\alpha}{\partial t} + \nabla\cdot(\alpha\mathbf{u}) = 0. \tag{3}$$

Volume-Of-Fluid method (VOF), defined by equations (1)-(3) is mass conservative, computationally efficient and flexible for treating complex interface shapes. Therefore, the VOF-method is a popular and powerful tool for the direct numerical simulation of immiscible two-phase flow.

2.1. Advection of indicator function

By its definition, the indicator function has the form of a step function in the continuum limit, while numerical approximation of convective terms in equations (1), (3) leads to smear function jump. Let us distinguish among the others two general approaches to deal with this problem. One of them is using low-dissipative second order scheme with Van-Leer limiter for approximation of convective terms, the other is an introduction of artificial compression term.

The last approach leads to the following form of advection equation (3):

$$\frac{\partial\alpha}{\partial t} + \nabla\cdot(\alpha\mathbf{u}) + \nabla\cdot(\alpha(1-\alpha)\mathbf{u}_{\mathrm{r}}) = 0, \tag{4}$$

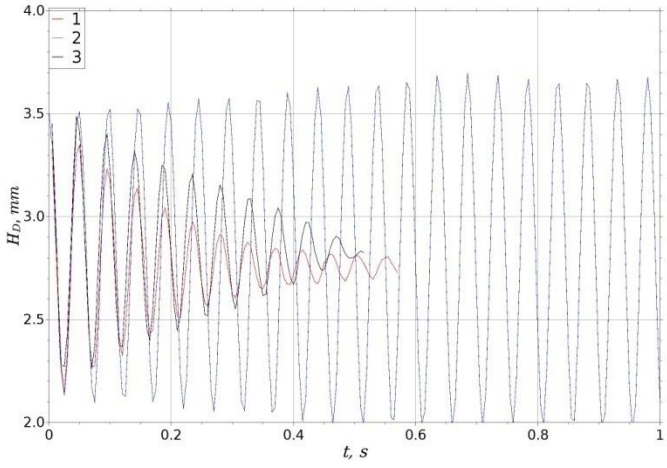

Figure 2. Calculated drop height H_D: 1- $C_\psi = 0.05$; 2 - $C_\psi = 0.01$; 3 - without any filtration and smoothing $C_{\text{fc}} = C_\psi = 0$.

where $\mathbf{u}_{\text{r}}$ is a compression velocity, the value of which is based on the scaled maximum fluid velocity magnitude in the transition region.

2.2. Calculation of interface curvature and normal vector

The solution of equation (4) updates the indicator function in such a way that the interface remains as sharp as possible. The reverse side of this is cumulative errors of capillary forces due to the unstable calculation of the normal vector and interface curvature.

For more accurate and stable calculation of the normal in cells near the interface, we first use smoothing of the indicator function procedure [5]. This is numerically done using the following relationship:

$$\alpha_{\text{s}}^{i+1} = C_{\text{fc}}\langle\langle\alpha_{\text{s}}^{i}\rangle_{\text{f}}\rangle_{\text{c}} + (1 - C_{\text{fc}})\alpha_{\text{s}}^{i},\ \ \alpha_{\text{s}}^{0} = \alpha,\ i = 0,1,\cdots,N \tag{5}$$

where the first operator $\langle\cdot\rangle_{\text{f}}$ means that the field values interpolated from the cell centers to the face centers and the second operator $\langle\cdot\rangle_{\text{c}}$ means that the field values at cell centers calculated by averaging values at face centers. A value of $C_{\text{fc}} = 0.5$ and $N = 2$ is used in present simulations.

The smoothed indicator function α_{s} is then used to obtain the interface normal vectors $\mathbf{n}_{\text{s}} = \nabla\alpha_{\text{s}}/|\nabla\alpha_{\text{s}}|$ at cell centers. The next step is to calculate interface curvature $K = \nabla\cdot\mathbf{n}_s$. In accordance with the control volume method, the divergence of the vector function is calculated as follows:

$$\nabla\cdot\mathbf{n}_{\text{s}} = \frac{1}{V_i}\sum_{f\in S_i}\left[\frac{\nabla\alpha_s}{|\nabla\alpha_s|}\right]_f\cdot\mathbf{S}_f,$$

where for each grid block *i*, V_i is its volume, S_i is set of its faces, $\mathbf{S}_f$ is the outward vector area of face.

Direct calculation of gradient $\nabla\alpha_{\text{s}}$ with subsequent normalization leads to nonzero vectors $\mathbf{n}_{\text{s}}$ outside the transition region. To deal with this problem, an extra filtration procedure is used for dummy face flux $\psi = \nabla\alpha_s\cdot\mathbf{S}$. This filtering will explicitly set the dummy fluxes ψ to zero when their magnitude is of the order of the numerical errors. The filtered flux reads:

$$\bar{\psi} = \psi - \max\ \ (\min\ \ (\psi,\psi_*),-\psi_*), \tag{6}$$

where ψ_* is a threshold value below which flux $\bar{\psi}$ is set to zero. The threshold value is chosen as $\psi_* = C_\psi|\mathbf{S}_f|\overline{|\nabla\alpha_s|}_f$, where $\overline{|\nabla\alpha_s|}_f$ is the average gradient magnitude over all faces where they are non-zero. The filtering coefficient should be chosen sufficiently small. In our simulations, we use $C_\psi = 0.01 \div 0.03$.

Once the interface curvature is computed, we smooth the calculated value in the direction normal to the interface, similar to that suggested in [6].

3. Results and discussion

First, we simulate a three-dimensional hemispherical water drop with a radius $R = 3.5$ mm on horizontal plane with contact angle $\theta = 90°$. The computational domain with dimensions $4R \times 4R \times$

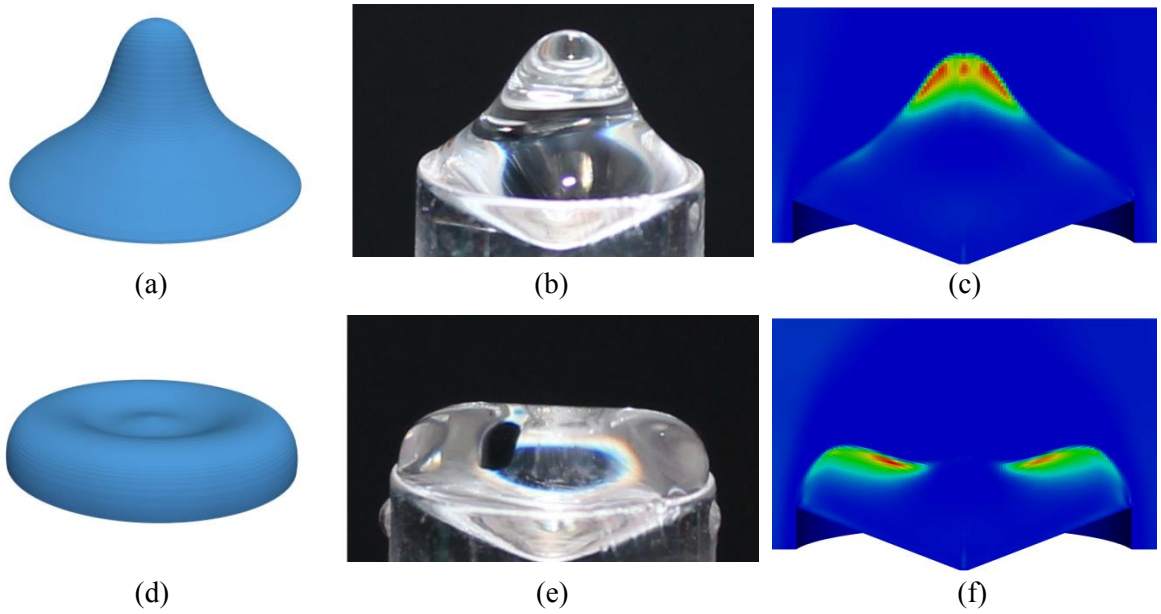

Figure 3. .Zonal oscillation mode (4,0). Calculated (a), (d) and observed (b), (e) free surface shape of the drop jointly with magnitude of the Umov–Poynting vector field (c), (e); when the phase of the oscillation (a)-(c) $\varphi = 0$, (d)-(f) $\varphi = \pi$.

$2R$ is discretized using a uniform Cartesian grid with a cell size $\delta\mathbf{x} = 0.05R$. At the time $t = 0$ volume gravity force is applied and the drop begins to oscillate, tending to the equilibrium form. Figure 2 shows the dynamics of a drop height depending on the parameters of smoothing (5) and filtration (6). One can see that more aggressive filtering practically does not accelerate convergence, but leads to underestimation of the drop height with respect to its theoretical value (2.8mm in accordance with [2]). The use of a low-dissipative numerical scheme for solving equation (4) without filtering and smoothing leads to the excitation of continuous solution oscillations.

Next, we consider a three-dimensional droplet of volume 87μl positioned on a cylindrical substrate as described above (figure 1). For this case, we carried out both an experimental study and numerical simulation.

The experiments were conducted with the use of a facility the detailed description of which is presented in [7]. The low-frequency vibrations of the substrate were generated by the speaker which was used as an electromechanical transducer. The vibrations of the speaker diaphragm were generated by alternating voltage supplied to the speaker coil by the amplifier of the signals of the signal generator.

The observed oscillation processes were recorded by digital camera Canon EOS 650D. The scene was lit by light emitting-diode lamps that were synchronized with the signal generator to achieve a stroboscopic effect. In the experiment, zonal mode (4.0) (figure 3, b, e) and tesseral mode (3,1) (figure 4, b, e) was obtained in the excitation frequency range from 38Hz to 45Hz. In the numerical experiments, the value of the substrate oscillation frequency was 40Hz.

Computational block-structured grid was generated by rotating an 2-D flat grid around the axe of symmetry to become a three-dimensional grid containing 1 752 500 hexagonal cells. Let us note that the final 3-D grid is symmetrical about the axis of rotation Oy, ensuring that the computed asymmetric flow comes from the physics and not an asymmetric grid topology.

It should be noted that in the numerical experiment it is necessary to initially introduce small asymmetry in the forcing vibrations of the substrate to achieve the non-axisymmetric (tesseral) mode of the drop oscillations.

Both the experimental and numerical drops experienced a similar free surface shapes (figures 3, 4) and close values of maximum and minimum drop heights H_D (table 1). Drop height was measured

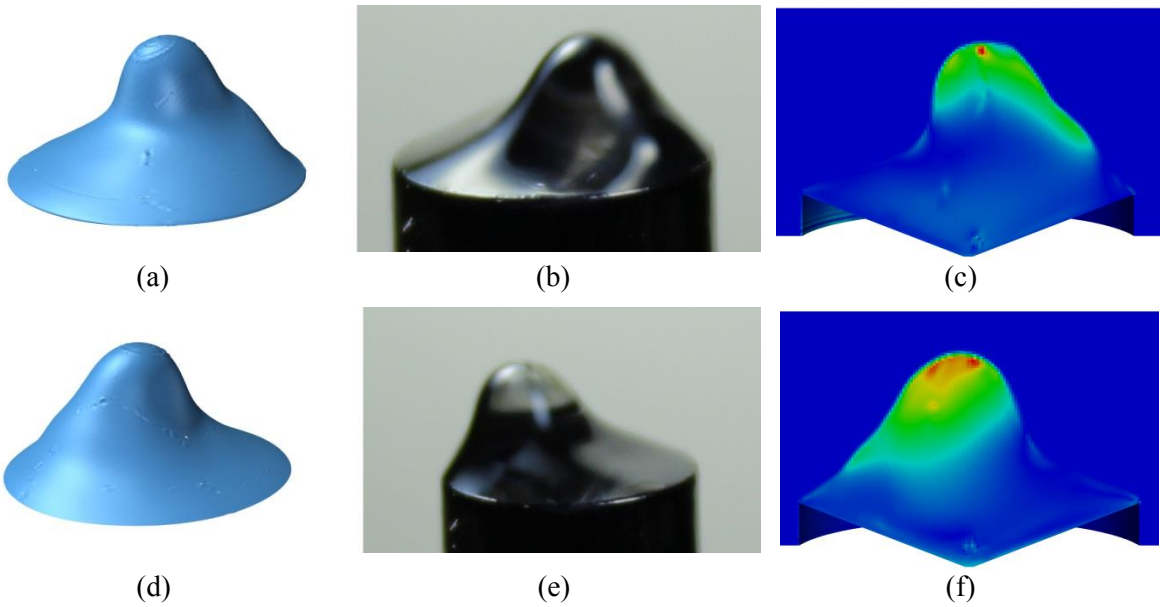

Figure 4. Tesseral oscillation mode (3,1). Calculated (a), (d) and observed (b), (e) free surface shape of the drop jointly with magnitude of the Umov–Poynting vector field (c), (e); when the phase of the oscillation (a)-(c) $\varphi = 0$, (d)-(f) $\varphi = \pi$.

from the top cross-section of the substrate.

For a more thorough analysis of the numerical solution, the Umov–Poynting vector field was constructed. The Umov–Poynting vector $\mathbf{S} = \mathbf{u}(p + \rho\mathbf{uu}/2)$ describes total energy flux in liquid. Figure 3, c, f and figure 4, c, f shows magnitude of the energy flux in the corresponding phase of oscillation. One can see that, for both zonal and tesseral modes, the most intense energy flow occurs at the top part of the drop near the interface surface.

Despite the pinning of the drop, the low-frequency eigenforms obtained in the experiment and reproduced by the numerical simulation are close to those shown in [8]. The developed numerical scheme allows to obtaining a detailed structure of microflows in an oscillating drop and contribution of a different mechanisms to the transition from one mode to another.

Table 1. Comparison of numerical values of H_D with experimental data.

	zonal mode (4,0)		tesseral mode (3,1)	
	max H_D, mm	min H_D, mm	max H_D, mm	min H_D, mm
Numerical results	3.72	1.81	3.25	1.95
Experimental data	3.70	1.78	3.23	1.91

Acknowledgments
The reported study was partially funded by RFBR according to the research project № 16-41-180276.

References

[1] Hirt C W and Nichols B D 1981 *Journal of Computational Physics* **39** 201
[2] Lubimov D V, Lubimova T P and Shklyaev S.V. 2006 *Physics of Fluids* **18** 012101
[3] Soh G Y, Yeoh G H and Timchenko V 2017 **21** 175
[4] Park Ch.-S, Kim H and Lim H.-Ch. 2016 *Experimental Thermal and Fluid Science* **78** 112

[5] Raeini A, Blunt M and Bijeljic B 2012 *Journal of Computational Physics* **231** 5653
[6] Shams M, Raeini A, Blunt M and Bijeljic B 2018 *Journal of Computational Physics* **357** 159
[7] Aleksandrov V, Kopysov S and Tonkov L 2018 *Microgravity Sci. Technol.* **30** 85
[8] Chang Ch.-T, Bostwick J B, Steen P H and Daniel S 2013 *Phys. Rev. E* **88** 023015